

Improving Small Lesion Segmentation in CT Scans using Intensity Distribution Supervision: Application to Small Bowel Carcinoid Tumor

Seung Yeon Shin^a, Thomas C. Shen^a, Stephen A. Wank^b, and Ronald M. Summers^a

^aImaging Biomarkers and Computer-Aided Diagnosis Laboratory, Radiology and Imaging Sciences, Clinical Center, National Institutes of Health, Bethesda, MD, USA

^bDigestive Disease Branch, National Institute of Diabetes and Digestive and Kidney Diseases, National Institutes of Health, Bethesda, MD, USA

ABSTRACT

Finding small lesions is very challenging due to lack of noticeable features, severe class imbalance, as well as the size itself. One approach to improve small lesion segmentation is to reduce the region of interest and inspect it at a higher sensitivity rather than performing it for the entire region. It is usually implemented as sequential or joint segmentation of organ and lesion, which requires additional supervision on organ segmentation. Instead, we propose to utilize an intensity distribution of a target lesion at no additional labeling cost to effectively separate regions where the lesions are possibly located from the background. It is incorporated into network training as an auxiliary task. We applied the proposed method to segmentation of small bowel carcinoid tumors in CT scans. We observed improvements for all metrics (33.5% \rightarrow 38.2%, 41.3% \rightarrow 47.8%, 30.0% \rightarrow 35.9% for the global, per case, and per tumor Dice scores, respectively.) compared to the baseline method, which proves the validity of our idea. Our method can be one option for explicitly incorporating intensity distribution information of a target in network training.

Keywords: Small lesion segmentation, intensity distribution, small bowel carcinoid tumor, computed tomography.

1. INTRODUCTION

Identifying small lesions from a computed tomography (CT) scan is clinically relevant since it can lead to immediate treatment if needed or trigger surveillance.¹ Despite its necessity, it is more difficult than for larger lesions since small lesions are likely to be less noticeable due to the relative lack of imaging features such as shape and texture as well as the size itself.

Especially in training a segmentation model for small lesions, it also entails a higher degree of class imbalance, which makes achieving a reasonable performance difficult. This issue can be mitigated by performing segmentation of an organ-of-interest, which could contain the target lesions, sequentially or jointly with lesion segmentation.^{2,3} Lung segmentation can benefit lung nodule segmentation by restricting the region of interest.² In the work by Tang et al.,³ liver and liver tumor segmentation is performed jointly using the same network to utilize the correlation between them. Features learned for liver segmentation would be relevant to liver tumor segmentation since the tumors reside within it.

In the work by Ayalew et al.,⁴ a significantly lower segmentation accuracy was achieved for segmenting tumors from an entire CT volume than conducting it from the identified liver, which may imply the need of restricting the region of interest for better small lesion segmentation. However, training the organ segmentation together with the target lesion segmentation requires additional ground-truth (GT) segmentations of the organ. Indeed, a clinician is interested in finding and marking abnormalities, but not an entire organ.

Further author information: Send correspondence to Seung Yeon Shin (seungyeon.shin@nih.gov) or Ronald Summers (rms@nih.gov)

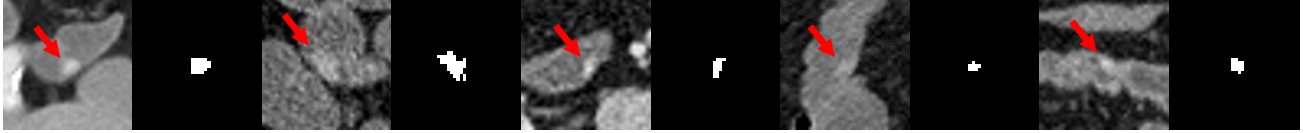


Figure 1: Examples of small bowel carcinoid tumors in our dataset. In each image, the tumor is pointed by the red arrow. Their corresponding ground-truth (GT) segmentation is also presented.

Intensity values in CT scans (Hounsfield units) carry important information and can provide clues as to which tissue a given voxel belongs to.⁵ An intensity distribution of a target lesion can be used to effectively separate regions where the lesions are possibly located from the other. It can be achieved by investigating intensity values within available GT segmentations of lesions, or can be provided as prior information.

We segment small bowel carcinoid tumors from CT scans in this paper. To the best of our knowledge, this is the first work that uses only CT scans for this task. In the work by Carlsen et al.,⁶ PET (positron emission tomography) / CT scans are used to segment tumors. Carcinoid tumor is a type of neuroendocrine tumor. Despite being rare (small bowel neoplasms including carcinoid tumors account for 0.5% of all cancers in the United States⁷), there has been an increase in the diagnosed incidence of carcinoid tumors for the past several decades. While more than half (50 – 71.4%) of carcinoid tumors develop within the gastrointestinal tract, they are found predominantly in the small bowel (24 – 44%).⁸ Figure 1 shows example carcinoid tumors in the small bowel. They are submucosal in location and often less than a centimeter in size.⁸ Like the aforementioned organ/lesion segmentation cases, performing small bowel segmentation together could help segmentation of small bowel carcinoid tumors. However, this is very costly due to the difficulty of labeling the small bowel.^{9–13}

Instead, we use the intensity distribution of small bowel carcinoid tumors to compute a probability of being tumor for each voxel. This soft label is provided to our segmentation model as an auxiliary task so that it can inform the model about our region of interest, which could contain carcinoid tumors, based on the intensity. It is a soft and possibly disconnected surrogate of the organ segmentation, which requires no additional annotation cost.

2. METHOD

2.1 Dataset

24 preoperative CT scans of 24 unique patients who underwent surgery and were found to have at least one carcinoid tumor within the small bowel were collected at our institution. They are all intravenous and oral contrast-enhanced abdominal CT scans. For each patient, either arterial phase ($n=18$) or venous phase ($n=6$) scans were selectively used according to the relevant description in the corresponding radiology report. All scans were acquired with oral administration of Volumen using 0.5, 1, or 2 mm slice thickness. They were cropped manually along the z-axis to include from the diaphragm through the pelvis. Then, they were resampled to have isotropic voxels of $1 \times 1 \times 1$ mm³.

GT segmentation of tumors was drawn in CT scans, using “Segment Editor” module in 3DSlicer,¹⁴ by referring to the corresponding radiology report as well as an available 18F-DOPA PET scan of each patient. This resulted in 88 annotated tumors in total. The tumor volume was 8 mm³ (approximately 2 mm diameter) at minimum and 1960 mm³ (approximately 16 mm diameter) at maximum. Figure 2 (a) shows the distribution of tumor sizes in our dataset.

2.2 Intensity Distribution Supervision

Figure 2 (b) shows the distribution of tumor intensities, which was computed by aggregating intensity values within the GT tumor segmentations in our dataset. Images that have been smoothed with anisotropic diffusion¹⁵ are used. Since the histogram is discontinuous around bin boundaries, to make a smooth function from it, kernel density estimation¹⁶ is performed using Gaussian kernels with automatic bandwidth determination. Finally, it is rescaled to have the maximum value of 1. The function in Figure 2 (b) is the constructed intensity likelihood model. It enables faster calculation of the likelihood for a large number of voxels than using the histogram.

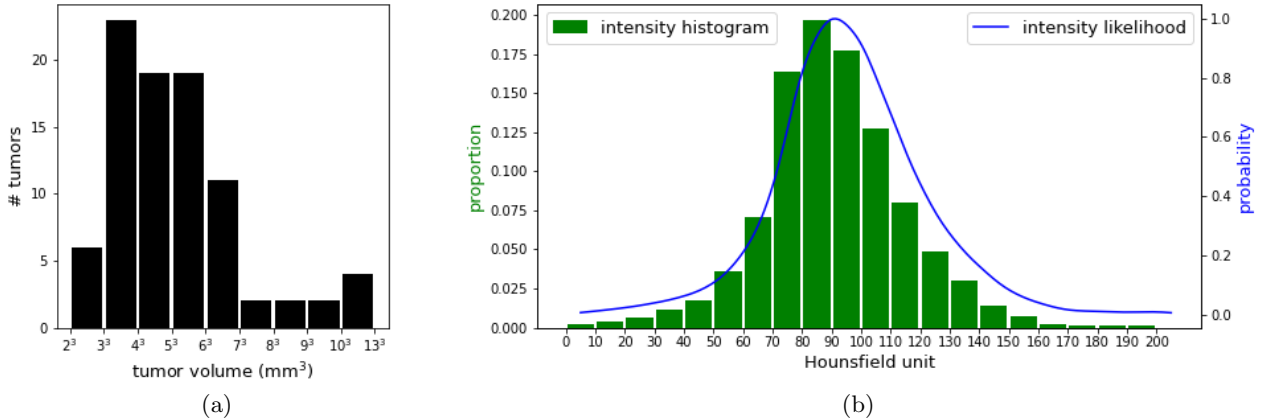


Figure 2: (a) Tumor volume distribution in our dataset. (b) Tumor intensity distribution (green) and a likelihood function (blue) built from it. They have different scales, so the left or right y-axis should be read for each. Refer to the text for the explanation of the likelihood function.

We note that the explained procedure requires no additional labeling effort. While it could be less precise, the likelihood model can be provided also from a user as prior information.

Figure 3 visualizes the network and data involved in training. Given an input volume X , a corresponding intensity likelihood volume Y_{IL} can be made using the prepared function, where each voxel value represents a probability of being tumor according to the intensity. Then, we make use of it to augment our tumor segmentation network. Similar to the network used by Tang et al.³ for joint liver and liver tumor segmentation, we use a network with two output channels in the proposed method. One channel predicts tumor segmentation. The second channel predicts the tumor intensity likelihood in place of organ segmentation. The generated likelihood volume Y_{IL} is used as supervision for this channel. This *soft* label is intended to inform the network about our region of interest, which could contain carcinoid tumors especially in terms of intensity, as *hard* organ segmentation supervision does in the joint organ/lesion segmentation case.³

2.3 Training

Two loss terms are involved in our network training (Figure 3), which are L_{seg} for tumor segmentation and L_{IL} for tumor intensity likelihood prediction. We use the generalized Dice loss¹⁸ for L_{seg} . For L_{IL} , a cross-entropy loss is used to measure the dissimilarity between GT and prediction of the tumor intensity likelihood. Finally, the overall loss function for training the proposed network is:

$$L = L_{seg} + \lambda L_{IL} \quad (1)$$

where λ is the relative weight for L_{IL} .

2.4 Evaluation Details

Our network architecture is based on that of the 3D U-Net,¹⁷ but has fewer channels, which are {8, 16, 32, 64}. While the final inference layer has 1x1x1 kernels, all the other convolution layers have 3x3x3 kernels. Group normalization¹⁹ is used between each convolution layer and non-linearity function. It is implemented using PyTorch 1.8.2.

We used an NVIDIA Tesla V100 32GB GPU to conduct experiments. For training, sub-volumes of size 224x224x224 sampled from the original volumes are used to fit in the memory. Each sub-volume is guaranteed to have at least one tumor. The mini-batch size was set as 1. We used the AdamW optimizer²⁰ and a weight decay of 5×10^{-4} . Based on the grid search, 3×10^{-4} and 1 were chosen for the learning rate and λ , respectively. For data augmentation, we opted to only use image rotation by 180° around the z-axis, which could simulate

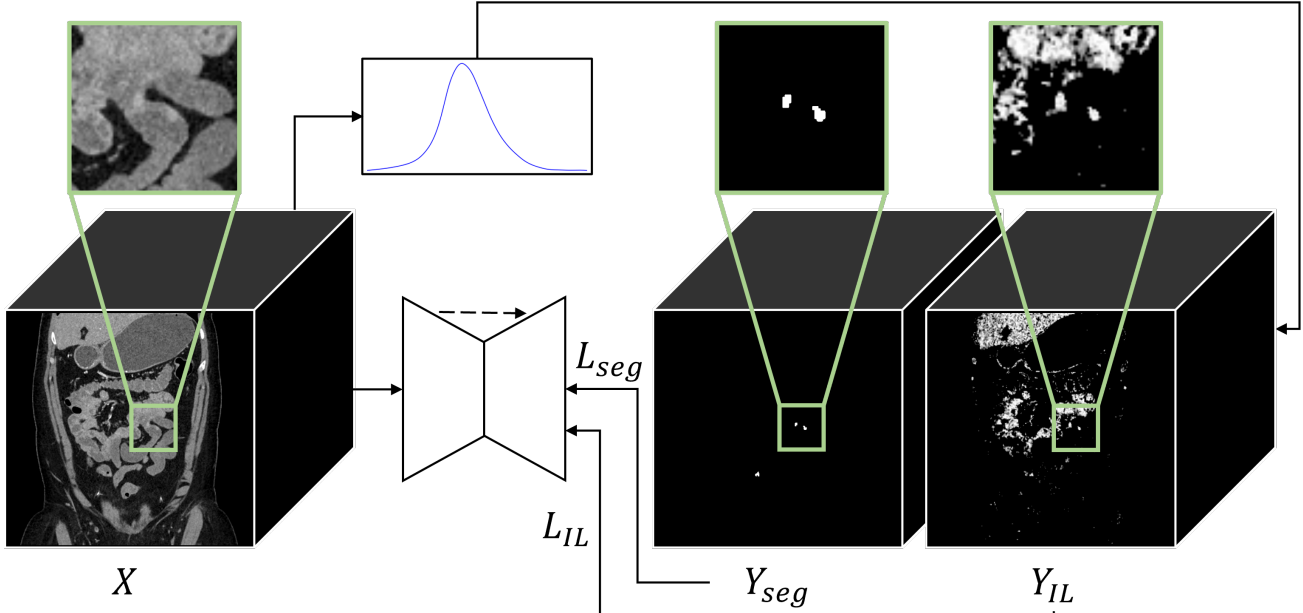


Figure 3: Visualization of data involved in training. An example input volume X and corresponding GT labels Y_{seg} , Y_{IL} for training are presented. Y_{seg} and Y_{IL} are GT tumor segmentation and GT intensity likelihood, respectively. Y_{IL} is generated from the input volume X using the likelihood function of Figure 2 (b), at no additional labeling cost. The network architecture is based on the structure of the 3D U-Net.¹⁷ The dotted line represents skip connections. The network predicts two outputs, namely, tumor segmentation and tumor intensity likelihood. They are compared against GT labels Y_{seg} and Y_{IL} to compute their respective losses L_{seg} and L_{IL} .

the supine and prone positions, after performing an investigation on the effects of more augmentation methods including image scaling.

We used a five-fold cross validation to utilize all scans for evaluation. In addition to the global Dice and per case Dice scores used in the work by Tang et al.,³ we calculate per tumor Dice scores for all tumors and for relatively larger tumors ($\geq 125 \text{ mm}^3$, which is approximately $\geq 6 \text{ mm}$ diameter) as well. While the per case Dice score denotes an average Dice score per scan/volume, the global Dice score is one computed by combining all CT scans into one. On the other hand, tight local image volumes around each tumor were taken into account to calculate the per tumor Dice scores. Also, paired t-tests are conducted to show the statistical significance of the proposed method.

3. RESULTS

3.1 Quantitative Evaluation

Table 1 provides quantitative results of different methods, especially in terms of different ways of using the tumor intensity distribution information. Applying a post processing to the prediction of the tumor segmentation network, where the intensity likelihood volume Y_{IL} is multiplied with the network predicted probability map, rather worsened the performance ('Seg + PP'). This may be because it could oversimplify rule out tumors that have intensity values deviating from the built intensity model. We also tried using the intensity likelihood volume as an additional input channel instead of as an additional output channel ('Seg + IL(in)'). It can be another way to highlight our region of interest at input level. However, it performed on par with the baseline that does not use this additional input channel, 'Seg'. On the other hand, the proposed method, 'Seg + IL', showed clear improvements for all types of Dice score when compared to the baseline. We note that the proposed method of using intensity distribution supervision does not entail any additional labeling effort. It can be included in training by looking up already available CT scans and corresponding GT tumor segmentation to define the tumor intensity likelihood model.

Table 1: Quantitative comparison of different methods. ‘Seg’ denotes performing only tumor segmentation from input CT volumes; ‘Seg + PP’ denotes applying a post processing (PP) that is based on the tumor intensity likelihood to the results of ‘Seg’; ‘Seg + IL(in)’ denotes using the generated likelihood volume as an additional input channel instead of as an additional output channel; ‘Seg + IL’ denotes the proposed method; ‘Seg + IL(shifted)’ denotes the proposed method but using a shifted likelihood function, which would be irrelevant with our target tumor. Dice scores were calculated at different subject levels, namely, global, per case, and per tumor. Refer to the text for the explanation on each of the metrics. Mean and standard deviation values are presented together, except for the global Dice scores. P-values are computed by conducting paired t-tests between the proposed method and the others with the Dice scores.

Method	Global	Per case		Per tumor		Per tumor ($\geq 125 \text{ mm}^3$)	
	Dice (%)	Dice (%)	p-value	Dice (%)	p-value	Dice (%)	p-value
Seg ¹⁷	33.5	41.3 \pm 27.2	0.0022	30.0 \pm 36.7	0.0398	37.7 \pm 36.4	0.1002
Seg + PP	27.8	36.2 \pm 25.3	0.0001	24.7 \pm 32.5	0.0005	30.5 \pm 31.3	0.0026
Seg + IL(in)	31.4	41.6 \pm 29.2	0.0860	32.8 \pm 39.0	0.1885	37.9 \pm 38.3	0.2133
Seg + IL	38.2	47.8 \pm 29.6	-	35.9 \pm 40.0	-	42.6 \pm 39.5	-
Seg + IL(shifted)	29.8	41.1 \pm 30.4	0.0084	30.1 \pm 38.3	0.0296	32.4 \pm 37.7	0.0025

We also investigate the effect of having the precise intensity model of targets. ‘Seg + IL(shifted)’ follows the proposed method but uses another likelihood function that is +100 shifted from the original one. The shifted function does not reflect the actual intensity distribution of our target tumor any more. It performed rather worse than the baseline.

The Dice scores in Table 1 tend to be low since carcinoid tumors in our dataset are small (Figure 2). Even small numbers of false positive and false negative voxels have a big impact on the Dice score of small lesions. Nevertheless, the proposed method showed clear improvements compared to the baseline. All methods including the proposed method showed higher Dice scores for relatively larger tumors ($\geq 125 \text{ mm}^3$, which is approximately $\geq 6 \text{ mm}$ diameter) than for all tumors.

3.2 Qualitative Evaluation

Figure 4 shows example segmentation results of small bowel carcinoid tumor. Compared to the baseline method that is trained without the intensity distribution supervision, the proposed method segments the entire tumor area better (first row), or segments more tumors (second and third rows). The last row represents a failure case, where the proposed method missed a blurry small tumor. Figure 5 presents an example result in 3D. While both of the baseline and the proposed methods segment the GT tumor successfully, the proposed method has less false positive segmentation.

4. CONCLUSION

We have presented a method for improving small lesion segmentation in CT scans, which utilizes intensity distribution of the target lesion. It requires no additional labeling effort. We applied the proposed method to segmentation of small bowel carcinoid tumors, and the experimental results proved the validity of our idea. The improved method could better assist a radiologist with the challenging task of finding carcinoid tumors in the small bowel on CT scans. In future work, we plan to apply the method to different target lesions to further validate the efficacy of the proposed method.

ACKNOWLEDGMENTS

This research was supported by the Intramural Research Program of the National Institutes of Health, Clinical Center. The research used the high performance computing facilities of the NIH Biowulf cluster.

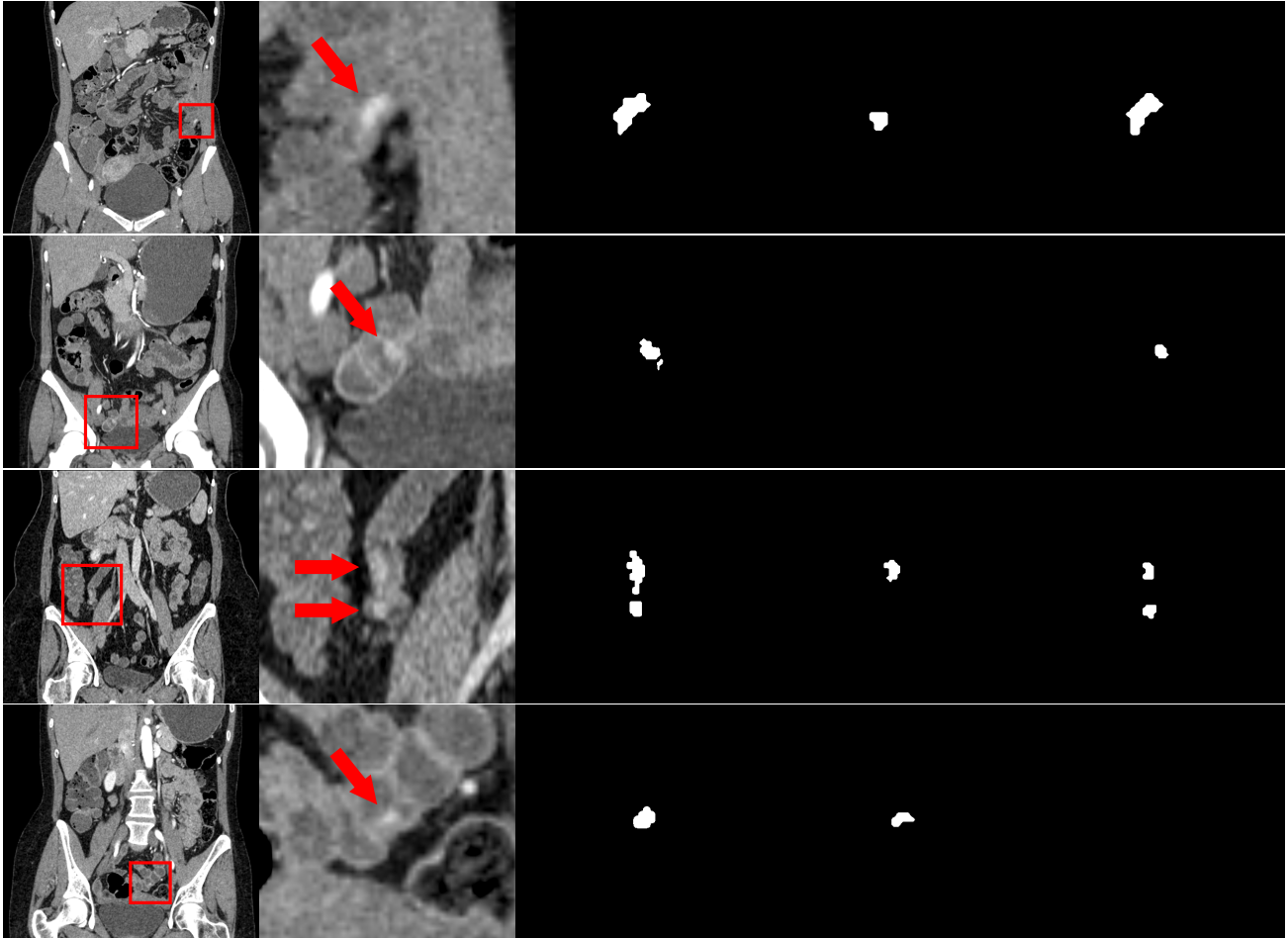


Figure 4: Example segmentation results of small bowel carcinoid tumor. Each row represents different cases. The columns, from left, represent input CT scan, zoomed view of the red box in the CT scan (The tumors are pointed by the red arrow), corresponding GT tumor segmentation, result of the baseline method ('Seg' in Table 1), and result of the proposed method ('Seg + IL' in Table 1), respectively.

REFERENCES

- [1] Cai, J., Tang, Y., Yan, K., Harrison, A. P., Xiao, J., Lin, G., and Lu, L., "Deep lesion tracker: Monitoring lesions in 4d longitudinal imaging studies," in *[2021 IEEE/CVF Conference on Computer Vision and Pattern Recognition (CVPR)]*, 15154–15164 (2021).
- [2] Kamble, B., Sahu, S. P., and Doriya, R., "A review on lung and nodule segmentation techniques," in *[Advances in Data and Information Sciences]*, Kolhe, M. L., Tiwari, S., Trivedi, M. C., and Mishra, K. K., eds., 555–565, Springer Singapore, Singapore (2020).
- [3] Tang, Y., Tang, Y., Zhu, Y., Xiao, J., and Summers, R. M., "E²Net: An edge enhanced network for accurate liver and tumor segmentation on ct scans," in *[Medical Image Computing and Computer Assisted Intervention – MICCAI 2020]*, Martel, A. L., Abolmaesumi, P., Stoyanov, D., Mateus, D., Zuluaga, M. A., Zhou, S. K., Racoceanu, D., and Joskowicz, L., eds., 512–522, Springer International Publishing, Cham (2020).
- [4] Ayalew, Y. A., Fante, K. A., and Mohammed, M. A., "Modified u-net for liver cancer segmentation from computed tomography images with a new class balancing method," *BMC Biomedical Engineering* **3**(1), 1–13 (2021).

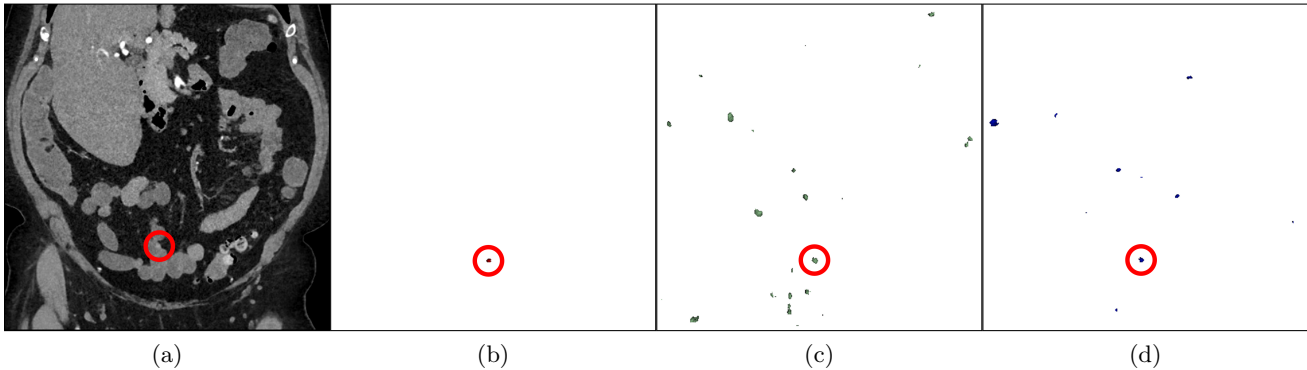


Figure 5: Example segmentation results in 3D. (a) Input CT scan that has one small bowel carcinoid tumor, which is highlighted by the red circle. An image slice in coronal view is shown. (b) GT segmentation. (c) Result of the baseline method (‘Seg’ in Table 1). (d) Result of the proposed method (‘Seg + IL’ in Table 1).

- [5] Buzug, T. M., “Computed tomography,” in [*Springer handbook of medical technology*], 311–342, Springer (2011).
- [6] Carlsen, E. A., Lindholm, K., Hindsholm, A., Gæde, M., Ladefoged, C. N., Loft, M., Johnbeck, C. B., Langer, S. W., Oturai, P., Knigge, U., et al., “A convolutional neural network for total tumor segmentation in [64cu] cu-dotatate pet/ct of patients with neuroendocrine neoplasms,” *EJNMMI research* **12**(1), 1–10 (2022).
- [7] Jasti, R. and Carucci, L. R., “Small bowel neoplasms: A pictorial review,” *RadioGraphics* **40**(4), 1020–1038 (2020). PMID: 32559148.
- [8] Hughes, M. S., Azoury, S. C., Assadipour, Y., Straughan, D. M., Trivedi, A. N., Lim, R. M., Joy, G., Voellinger, M. T., Tang, D. M., Venkatesan, A. M., et al., “Prospective evaluation and treatment of familial carcinoid small intestine neuroendocrine tumors (si-nets),” *Surgery* **159**(1), 350–357 (2016).
- [9] Shin, S. Y., Lee, S., Elton, D., Gulley, J. L., and Summers, R. M., “Deep small bowel segmentation with cylindrical topological constraints,” in [*Medical Image Computing and Computer Assisted Intervention – MICCAI 2020*], Martel, A. L., Abolmaesumi, P., Stoyanov, D., Mateus, D., Zuluaga, M. A., Zhou, S. K., Racoceanu, D., and Joskowicz, L., eds., 207–215, Springer International Publishing, Cham (2020).
- [10] Shin, S. Y., Lee, S., and Summers, R. M., “Unsupervised domain adaptation for small bowel segmentation using disentangled representation,” in [*Medical Image Computing and Computer Assisted Intervention – MICCAI 2021*], de Bruijne, M., Cattin, P. C., Cotin, S., Padoy, N., Speidel, S., Zheng, Y., and Essert, C., eds., 282–292, Springer International Publishing, Cham (2021).
- [11] Shin, S. Y., Lee, S., and Summers, R. M., “A graph-theoretic algorithm for small bowel path tracking in CT scans,” in [*Medical Imaging 2022: Computer-Aided Diagnosis*], Drukker, K., Iftexharuddin, K. M., Lu, H., Mazurowski, M. A., Muramatsu, C., and Samala, R. K., eds., **12033**, 863 – 868, International Society for Optics and Photonics, SPIE (2022).
- [12] Shin, S. Y., Lee, S., and Summers, R. M., “Graph-based small bowel path tracking with cylindrical constraints,” in [*2022 IEEE 19th International Symposium on Biomedical Imaging (ISBI)*], 1–5 (2022).
- [13] Shin, S. Y. and Summers, R. M., “Deep reinforcement learning for small bowel path tracking using different types of annotations,” (2022).
- [14] Fedorov, A., Beichel, R., Kalpathy-Cramer, J., Finet, J., Fillion-Robin, J.-C., Pujol, S., Bauer, C., Jennings, D., Fennessy, F., Sonka, M., Buatti, J., Aylward, S., Miller, J. V., Pieper, S., and Kikinis, R., “3d slicer as an image computing platform for the quantitative imaging network,” *Magnetic Resonance Imaging* **30**(9), 1323 – 1341 (2012). Quantitative Imaging in Cancer.
- [15] Black, M., Sapiro, G., Marimont, D., and Heeger, D., “Robust anisotropic diffusion,” *IEEE Transactions on Image Processing* **7**(3), 421–432 (1998).
- [16] Parzen, E., “On Estimation of a Probability Density Function and Mode,” *The Annals of Mathematical Statistics* **33**(3), 1065 – 1076 (1962).

- [17] Çiçek, Ö., Abdulkadir, A., Lienkamp, S. S., Brox, T., and Ronneberger, O., “3d u-net: Learning dense volumetric segmentation from sparse annotation,” in [*Medical Image Computing and Computer-Assisted Intervention – MICCAI 2016*], Ourselin, S., Joskowicz, L., Sabuncu, M. R., Unal, G., and Wells, W., eds., 424–432, Springer International Publishing, Cham (2016).
- [18] Sudre, C. H., Li, W., Vercauteren, T., Ourselin, S., and Jorge Cardoso, M., “Generalised dice overlap as a deep learning loss function for highly unbalanced segmentations,” in [*Deep Learning in Medical Image Analysis and Multimodal Learning for Clinical Decision Support*], Cardoso, M. J., Arbel, T., Carneiro, G., Syeda-Mahmood, T., Tavares, J. M. R., Moradi, M., Bradley, A., Greenspan, H., Papa, J. P., Madabhushi, A., Nascimento, J. C., Cardoso, J. S., Belagiannis, V., and Lu, Z., eds., 240–248, Springer International Publishing, Cham (2017).
- [19] Wu, Y. and He, K., “Group normalization,” in [*Proceedings of the European Conference on Computer Vision (ECCV)*], (September 2018).
- [20] Loshchilov, I. and Hutter, F., “Decoupled weight decay regularization,” in [*International Conference on Learning Representations*], (2019).